RGNZ/MGPB

Surface Roughness Assessment of Natural Rock Joints Based on an Unsupervised Pattern Recognition Technique Using 2D Profiles

Rudarsko-geološko-naftni zbornik
(The Mining-Geology-Petroleum Engineering Bulletin)
UDC: 622.2
DOI: 10.17794/rgn.2023.2.14

Original scientific paper

Ali Mohamad Pakdaman[1], Mahdi Moosavi[2]

[1] *School of Mining Engineering, College of Engineering, University of Tehran, Tehran, Iran, E-mail address: a.pakdaman@ut.ac.ir.*

[2] *School of Mining Engineering, College of Engineering, University of Tehran, Tehran, Iran, (corresponding author), E-mail address: mmoosavi@ut.ac.ir.*

Abstract

The stability of a jointed rock mass is generally controlled by its shear strength that significantly depends on surface roughness. So far, different methods have been presented for determining surface roughness using 2D profiles. In this study, a new method based on the unsupervised pattern recognition technique using a combination of statistical, geostatistical, directional, and spectral methods for the quantification of the surface roughness will be proposed. To reach this goal, more than 10,000 profiles gathered from 92 surfaces of natural rock joints were scanned. The samples were collected from limestone cores of the Lar Dam located in the Mazandaran Province, Iran. After introducing a new spectral index, determined from the fast Fourier transform for measuring the unevenness of rough profiles, statistical, geostatistical, directional, and spectral features revealing waviness and unevenness of the 2D profiles were extracted, and a representative vector and profile for each surface were introduced through the weighted mean and median of the profile features. Principal component analysis (PCA) was utilized for finding the direction of the maximum variance of information. Then, clustering of the 92 samples was performed via K-means, and the silhouette measure was used in order to find the optimal number of clusters resulted in the creation of 13 clusters. To verify the procedure, a sample was selected in each cluster, and direct shear tests were performed on the samples. Comparing the experiments and the clustering results shows they are in good agreement. Thus, the method is an efficient tool for the quantitative recognition of surface roughness considering the waviness and unevenness of a surface.

Keywords:

joint roughness coefficient; joint shear strength; pattern recognition; clustering; principal component analysis

1. Introduction

The shear strength of rock joints is an important factor controlling the stability of a jointed rock mass. So far, different models have been proposed in order to determine the shear strength of rough surfaces. The evaluation of surface roughness in these models can be generally categorized into two groups. In the first group, the evaluation of surface roughness is performed using 2D profiles (**Patton, 1966; Ladanyi, and Archambault, 1970; Barton and Choubey, 1977; Kulatilake et al., 1995; Zhao, 1997**) while in the second group, 3D surface assessment is performed via the creation of a 3D network on the rough surface (**Grasselli et al., 2002; Xia et al., 2014; Tang and Wong, 2015; Yang et al., 2016; Zhang et al., 2016; Liu et al., 2017**). Although the latter yields a more precise illustration of a rough surface, it is more difficult and time-consuming. Furthermore, in lots of in situ studies, the use of the method is neither practical nor affordable. In contrast, the application of 2D profiles due to their simplicity is preferred in practice.

Among the 2D criteria, the Barton model is probably the most popular one for determining the shear strength of discontinuities (**ISRM, 1978**). However, the shear strength derived from the model can be highly variable due to the subjective selection of the joint roughness coefficient (JRC) for the 2D profiles. Moreover, no clear procedure was presented for the selection of the representative profile(s) in each surface in order to be compared with the standard ones.

So far, different methods have been used for the quantitative determination of surface roughness. Statistical methods have been applied for the assessment of the JRC (**Tse and Cruden, 2019; Yu and Vayssade, 1991; Yang et al., 2001(b); Gao et al., 2015; Jang et al., 2014; Li and Zhang, 2015; Zhang et al., 2014**). In these methods, a relation is made between the JRC of 2D profiles and statistical parameters commonly attained based on Barton's standard profiles. Also, surface roughness has been quantified using fractal geometry (**Mandelbrot, 1983**). The most important fractal methods for

Corresponding author: Mahdi Moosavi
e-mail address: mmoosavi@ut.ac.ir

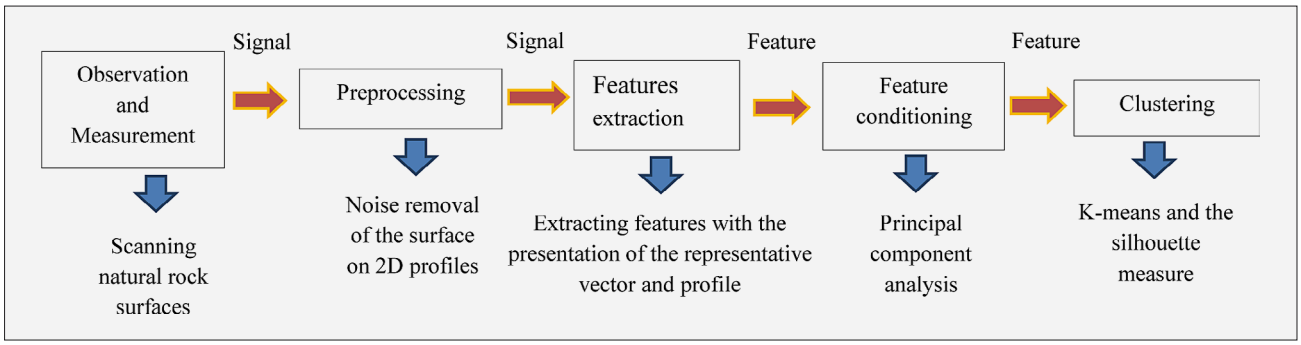

Figure 1: The unsupervised pattern recognition procedure

evaluating surface roughness are the divider (**Poon et al., 1992; Lee et al., 1990; Bae et al., 2011**), box counting (**Feder, 1988; Jansson, 2006; Pierra et al., 2005**), h-L method (**Xie and Pariseau, 1994; Askari and Ahmadi, 2007**), variogram (**Kulatilake, 1998**), spectral (**Shirono and Kulatilake, 1997**), line scaling (**Kulatilake et al., 1997**), and roughness-length methods (**Kulatilake and Um, 1999**). In addition, the application of geostatistical methods for surface morphology recognition has widely been extended (**Roko et al., 1997; Lianheng et al., 2018; Chen et al., 2015**). The studies stated a direct relationship between the JRC and the slope of the semivariogram of the profile heights. On the other hand, with the vast use of Grasselli's model (**Grasselli and Egger, 2003**), the concept of directional roughness has been implemented in 2D profiles (**Tatone and Grasselli, 2010**). More recently, spectral methods which are generally based on the Fourier series (**Ueng and Chang, 1990; Yang et al., 2001; Sun et al., 1988; Yong et al., 2018**), the Fourier transform (**Pickerin and Aydin, 2015**), the wavelet transform (**Asadi et al., 2015**), and the power spectral density (**Wang et al., 2019**) have been utilized for the evaluation of the joint roughness.

Magsipoc et al. (2020) gathered 2D and 3D surface roughness quantification methods that are based on statistical, fractal, and directional characterization of rough surfaces. Recently, **Barton et al. (2023)** reviewed joint roughness and its influence on the shear strength of rock joints while elaborating on issues related to the application of this parameter to rock engineering problems. In another research study, **Kulatilake and Ankah (2023)** studied the current status of contact and non-contact methods utilized for the surface assessment of rock joints.

The determination of surface roughness based on only a single parameter due to its complexity does not seem to be sufficient. In other words, the waviness and unevenness of a 2D profile ought to be properly described via different factors. Recent studies have focused on the application of more than one parameter for the description of a rough surface (**Zhang et al., 2014; Gao et al., 2015; Wang et al., 2017; Wang et al., 2019; Fathipour-Azar, 2021**).

Sampling interval plays an important role for joint roughness estimation when joint surfaces are scanned using discrete points (**Yu and Vayssade, 1991; Tatone and Grasselli, 2010, 2013; Yong et al., 2018; Ankah et al., 2022**). It is well understood that decreasing a sampling interval will result in a rougher surface estimation (**Kulatilake and Ankah, 2023; Barton et al., 2023**). Furthermore, the scale effect is another factor that impacts roughness evaluation. While some studies reported a negative scale effect (reducing roughness and shear strength) as a result of increasing the joint size, the others stated a positive scale effect (**Tatone and Grasselli, 2013; Barton et al., 2023**). **Kulatilake and Ankah (2023)** declared that roughness heterogeneity is the most crucial reason controlling this important effect.

The objective of this research is to recognize surface roughness based on 2D profiles using an unsupervised pattern recognition technique. To do so, statistical, geostatistical, directional, and spectral features revealing waviness and unevenness of the profiles will be used for an appropriate description of surface roughness. In this way a new spectral index is introduced for measuring the unevenness of rough profiles. Additionally, a quantified method for the identification of the representative surface features and profile will be proposed. Then, the rock surfaces are clustered based on the features gained from the 2D profiles, so this method not only leads to the quantitative recognition of surface roughness but also limits performing tests to a few samples representing the features of clusters. To verify the procedure, experimental tests will be performed in order to be compared with the pattern recognition results.

2. Methodology

In lots of civil structures excavated in a rock mass, numerous rock cores intersecting discontinuities having different roughness levels exist. In practice, performing the direct shear test on all the samples is neither possible nor affordable. Therefore, clustering the cores based on their roughness level and performing the test only on a few samples representing the clusters not only reduces the cost of the tests but also causes proper recognition of the surface roughness of the samples.

Pattern recognition is a procedure for classification and clustering based on measurement and observation.

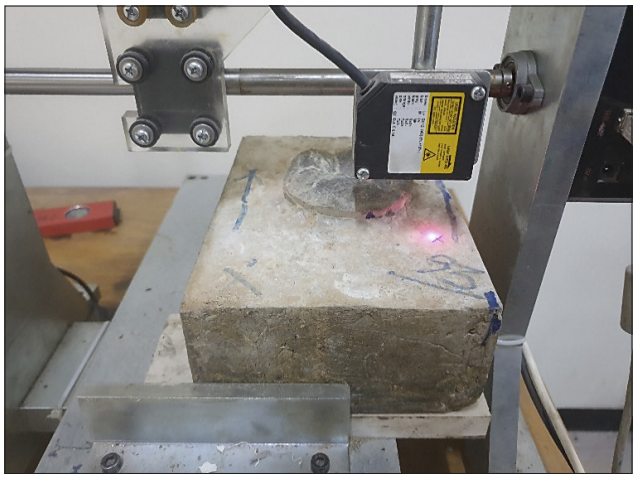

Figure 2: A prepared sample for scanning the rough surface

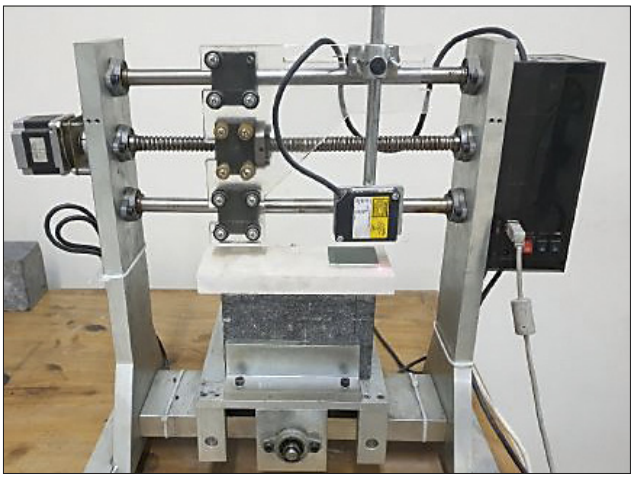

Figure 3: The scanning device

The general procedure of unsupervised pattern recognition adapted for the surface recognition of rock joints is illustrated in **Figure 1** (**Duda et al., 2001**). Firstly, scanning of the rock surfaces and preparing profiles are performed. Then, statistical, geostatistical, directional, and spectral features are extracted from 2D profiles, and a unique vector of features as well as a profile will be introduced to each surface called "the representative vector and profile", respectively. Next, principal component analysis (PCA) is applied for reducing overlaps between the features and observing the directions of maximum distribution of information. Finally, surfaces are clustered via K-means, and the optimal number of clusters is found by the silhouette measure.

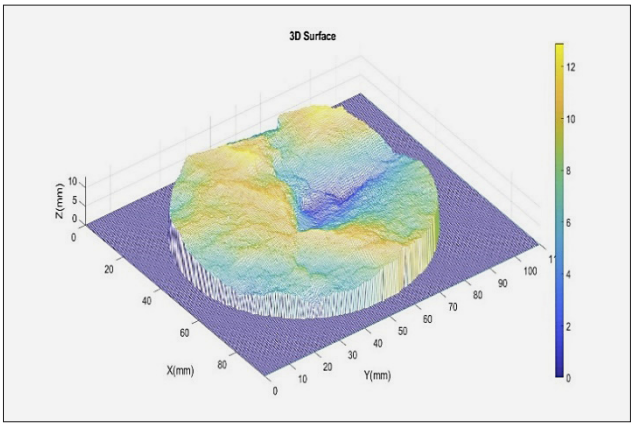

Figure 4: The reconstructed surface

3. Sample Preparation and Surface Scan

92 natural joint samples were gathered from limestone cores of the Lar Dam located in the Mazandaran Province, Iran. Natural fractures not only help to present a realistic recognition of rock surfaces but they can also provide a broad range of surface roughness. The rock fractures were selected such that they have no fillings. In addition, an attempt was made to choose those with the least surface weathering though this effect is an inseparable part of natural fractures. The shortest diameters of samples are 85 mm (PQ) and 63.5 mm (HQ) while the longest diameters range from 63.5 to 100.23 mm. From a lithological point of view, the samples were collected from limestone layers.

During the preparation of the rock samples, two ends of the surface were cut in the direction of the natural fracture to keep the fracture surface horizontal (**Muralha et al., 2014**). Then, the lower part was put in a mold and cement grout with a water-to-cement ratio (W/C) equal to 40 percent was added. In order to prevent cracking, a chemical additive with the ratio of 0.5 percent to cement was used. **Figure 2** shows a prepared sample.

Joint surfaces were scanned using a laser scanner frame developed in the rock mechanics laboratory at the

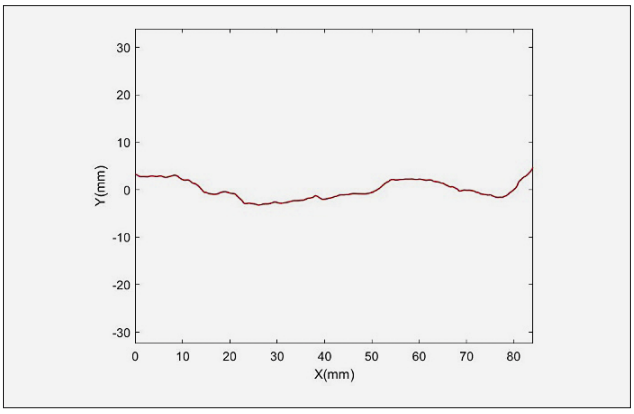

Figure 5: A generated profile of the surface in the shear direction

University of Tehran (see **Figure 3**). The precision of the laser scanner was 0.02 mm, and the sampling interval was set at 0.5 mm in two perpendicular directions (x and y directions, as shown in **Figure 4**). Depending on the sample size, 110 to 160 profiles on each surface were reconstructed in an assumed shear direction (the direction of the longer diameter of the core) resulted in the generation of more than 10,000 profiles. As the values of

the profile features highly depend on the shear direction (**Magsipoc et al., 2020; Kulatilake and Ankah, 2023; Barton et al., 2023**), the purpose of assuming a specific shear direction is to calculate the features along it. In addition, validation tests will be performed in the same direction. **Figures 4 & 5** show a 3D scanned surface and a profile of the sample in the shear direction, respectively.

4. Feature Extraction

Feature selection plays a critical role in order to fulfill the goal of clustering. In this study, the goal is to cluster surfaces using 2D profiles based on their roughness level. Therefore, features having a definite relationship with roughness are selected. In this regard, statistical, geostatistical, directional, and spectral features selected for the pattern recognition procedure will be described in this section. Before the extraction of the features, profile coordinates are translated according to the mean line (the line with respect to which the sum of the positive and negative areas above and below the line is almost zero).

Three statistical parameters (δ, λ and Z_2 were selected (**Equations 1-3**)) based on their frequent applications in the prediction of JRC (**Li and Zhang, 2015**). Besides, the parameters give an insight into the waviness and unevenness of a profile.

$$\delta = \frac{L_t - L}{L} \tag{1}$$

$$\lambda = \frac{R_z}{L} \tag{2}$$

$$Z_2 = \left[\frac{1}{L}\int_{x=0}^{x=L}\left(\frac{dy}{dx}\right)^2 dx\right]^{1/2} = \left[\frac{1}{L}\sum_{i=1}^{N-1}\frac{\left(y_{i+1}-y_i\right)^2}{\left(x_{i+1}-x_i\right)}\right]^{1/2} \tag{3}$$

Where dx and dy are x and y increments of the profile (mm), respectively; N is the number of sampling points (dimensionless); L is the projected length of the profile in the x direction (mm); L_t is true length of the profile (mm); R_z is the maximum height of the profile (mm). Equations 1-3 reveal the fact that λ and Z_2 which are dimensionless parameters tend to show the waviness and unevenness of a profile, respectively, while δ which is the other dimensionless parameter is the combination of the both.

The semivariogram of the profile heights (**Equation 4**) is used in order to extract geostatistical features of a profile.

$$\gamma(h) = \frac{1}{2N(h)}\sum_{i=1}^{N(h)}\left\{y(x_i) - y(x_i+h)\right\}^2 \tag{4}$$

Where $y(x_i)$ and $y(x_i+h)$ are the height of a profile (mm) on the abscissa x_i and x_i+h, respectively; h ($h \in N^+$ which is a dimensionless factor) is the interval in which a paired sample is taken; $N(h)$ is the number of paired samples. The distance after which sample pairs behave independently is the Range (a_1), and the corresponding $\gamma(h)$ is the Sill (C_1+C_0). The Nugget (C_0) is the $\gamma(h)$ when $h \to 0$, and the Partial Sill C_1 is the difference between the Sill and Nugget (see **Figure 6**). In a geostatistical analysis, the experimental semivariogram is obtained based on the data points. Then, the theoretical semivariogram (the Gaussian model in this study because of its higher goodness of fit) is fitted in order to find the geostatistical parameters (C_1, C_0, a_1) (**Lianheng et al., 2018**). In this study, the units of $\gamma(h)$, C_1, C_0 are mm^2 while a_1 is a dimensionless parameter. Due to the fact that $\frac{C_1}{a_1}$ (which is determined in mm^2) has a direct relationship with the JRC (**Lianheng et al., 2018**), this parameter (implying waviness of a profile) was selected as a geostatistical feature for the pattern recognition procedure.

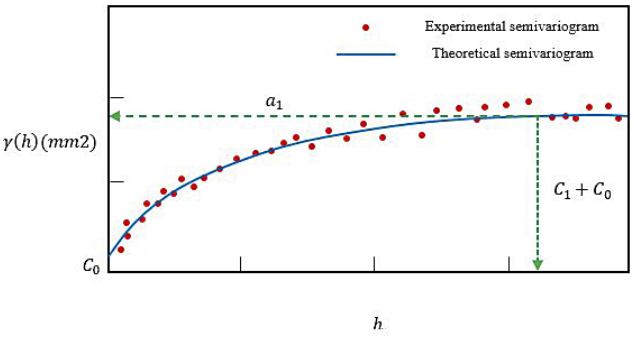

Figure 6: The semivariogram diagram

After a wide application of 3D directional models (**Grasselli et al., 2002; Grasselli and Egger, 2003**), the concept of directional roughness has been implemented in 2D profiles (**Tatone and Grasselli, 2010**). Accordingly, different threshold dips (θ^*) in the test direction are considered, and the sum of the profile segments with dips greater than the threshold divided by the total length of the profile is calculated as the L_θ^* (called normalized contact area). Then, by fitting **Equation 5** to the graph of $L_\theta^* - \theta^*$ (as depicted in **Figure 7**), the directional roughness parameter is acquired.

$$L_\theta^* = L_0\left(\frac{\theta_{\max}^* - \theta^*}{\theta_{\max}^*}\right)^C \tag{5}$$

Where L_0 is the normalized length of the profile facing the shear direction greater than an angular threshold 0°; $\theta_{\max}^*$ is the maximum slope angle of profile segments facing the shear direction (degrees); C is a dimensionless fitting parameter. $\left(\frac{\theta_{\max}^*}{1+C}\right)$ is selected as a directional roughness parameter (determined in degrees) for the surface assessment procedure. This parameter tends to show the unevenness of a rough profile.

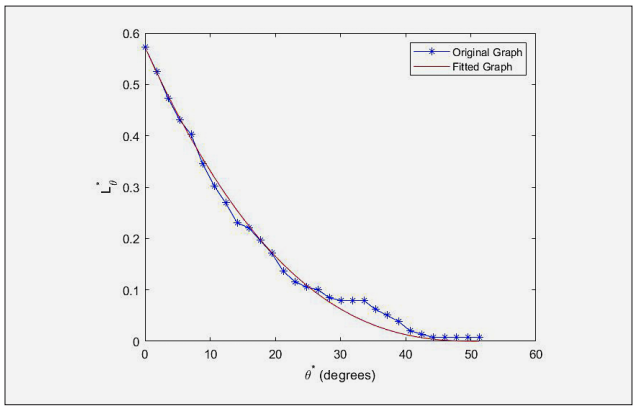

Figure 7: Relation between contact area (L^*_θ) and threshold dip (θ^*)

The transformation of rough profiles from distance to frequency domain helps to divulge precious information about a profile. In these techniques, each profile is treated as a signal, and various spectral transformation techniques such as the fast Fourier transform (FFT) and the power spectral density (PSD) are imposed on the profile (**Pickerin and Aydin, 2015; Wang et al., 2019**). After introducing a new spectral index $\left(\frac{\Delta L}{L_T}\right)_{FFT}$, achieved using the fast Fourier transform, another spectral feature (*Pf*), derived based on the power spectral density, is described for the quantification of roughness in 2D profiles.

Since roughness profiles are discrete, the fast Fourier transform (FFT) is used for the transformation. Since negative frequencies have no physical meaning, the single sided fast Fourier transform is obtained. Hence, after transforming the profile to the frequency domain, frequencies greater than a threshold (which is 0.1 1/mm in this study) will be removed. Then, a smooth profile will be created by applying the inverse form (see **Figure 8**). The difference between the true length (L_T) and the filtered true length ($(L_T)_{filtered}$) of the profile (**Equation 6**) was selected as a spectral feature for the pattern recognition technique. As can be observed in **Figure 8**, $\left(\frac{\Delta L}{L_T}\right)_{FFT}$ is related to the unevenness of a profile.

$$\left(\frac{\Delta L}{L_T}\right)_{FFT} = \frac{L_T - (L_T)_{filtered}}{L_T} \tag{6}$$

The power spectral density (PSD) function of a profile can be obtained by the calculation of the Fourier transform of the autocorrelation function of the profile. Similar to the Fourier transform, the single-sided power spectral density function is used. Wang et. al. introduced *Pf* (**Equation 7**) based on 112 roughness profiles having a definite relationship with the JRC as a spectral feature (**Wang et al., 2019**).

$$Pf = \left\{ \begin{array}{l} \sum_{n=0}^{n=\left(\frac{N}{2}\right)-1} A_n fr_n^{ave}; N = 2k \\ \sum_{n=0}^{n=\left(\frac{N-1}{2}\right)-1} A_n fr_n^{ave}; N = 2k \pm 1 \end{array} \right\} \tag{7}$$

Where fr_n^{ave} is the average frequency of the components between fr_n and $fr_{n+1}(1/mm)$; A_n is the average power of the profile in the frequency interval (mm^2); N is the number of sampling points (dimensionless). *Pf* (mm) was the other feature selected for the pattern recognition procedure implying the waviness of a profile.

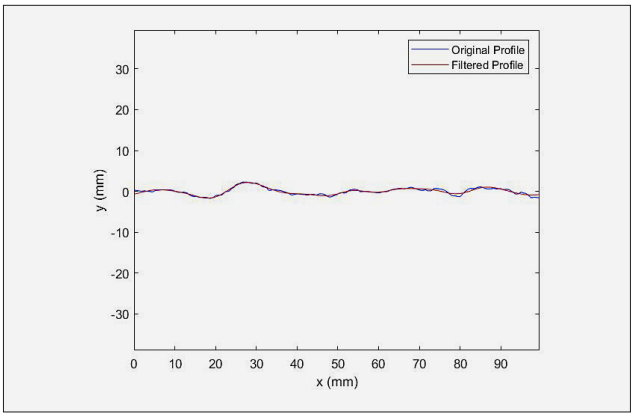

Figure 8: The tenth Barton standard profile and its filtered form

5. Feature Conditioning

The statistical, geostatistical, directional, and spectral analyses of a profile yield seven features for the pattern recognition procedure. The features are calculated for all the profiles of a surface in the shear direction. Feature conditioning including two main parts is explained here. First, the representative vector and profile of a surface are introduced. Then, principal component analysis (PCA) of the representative vectors is performed.

5.1. Representative Vector and Profile of a Surface

Two methods (weighted mean and median) are used in this research for the calculation of a representative vector and profile of a surface. In the first method, the weighted mean (μ_i) and the standard deviation (σ_i) of the features (f_i) on a surface are calculated using **Equations 8-10**.

$$w_j = \frac{L_j}{\sum_{k=1}^{M} L_k} \tag{8}$$

$$\mu_i = \frac{\sum_{k=1}^{M} w_k (f_i)_k}{\sum_{k=1}^{M} w_k} \tag{9}$$

$$\sigma_i = \sqrt{\frac{\sum_{k=1}^{M} w_k \left((f_i)_k - \mu_i \right)^2}{\left(\frac{M-1}{M} \right) \sum_{k=1}^{M} w_k}} \quad (10)$$

Where L_i and w_i are the projected length (mm) and weight (dimensionless) of the th profile of a surface; M is the number of profiles on a surface (dimensionless); f_i is the i^{th} feature of a profile vector; μ_i is the weighted mean of the i^{th} feature; σ_i is the standard deviation of the i^{th} feature on a surface (measurement units of f_i, μ_i, σ_i depend on the selected feature). Then, the outliers that are the profiles with ($f_i < \mu_i - 3\sigma_i$ *Or* $f_i > \mu_i + 3\sigma_i$) are removed. Finally, by recalculating the weighted mean and standard deviation of the features, the representative vector of a surface is defined.

In the second method, weighted medians of the profile features are calculated. Accordingly, the i^{th} feature of the profiles in a surface is arranged in ascending order, and the weighted median of a feature (f_k) is the one fulfilling **Equation 11** (**Cormen et al., 2001**).

$$\sum_{i=1}^{k-1} w_i \le \frac{1}{2} \; and \; \sum_{i=k+1}^{M} w_i \le \frac{1}{2} \quad (11)$$

The representative profile of a surface in the both methods is selected as the closest profile to the representative vector. In this way, Euclidean distance was utilized while prior to the calculation of the distance, the normalization of features and their representative values for each feature was performed for removing the scales. Despite the fact that in a significant portion of the scanned surfaces the representative profiles obtained from the weighted mean and median of the features were identical, in some surfaces the two were not matched.

5.2. Principal Component Analysis (PCA)

The selected features should be transformed so that their overlaps are reduced. Principal component analysis (PCA) is a linear transformation after which the features are uncorrelated, and the first few transformed features keep the most significant portion of information (see **Figure 9**). The PCA is carried out separately for the representative mean and median vectors of the surfaces. The procedure for the PCA is as follows (**Duda et al., 2001**):

Standard normalization of the representative vectors of 92 surfaces is performed by constructing the representative feature matrix (X), and the covariance matrix (Σ) of the normalized representative vectors is calculated. Then, eigenvalues and eigenvectors of the covariance matrix (Σ) are determined such that **Equation 12** is obtained.

$$\Sigma V = VD \quad (12)$$

Where D and V are the matrices of eigenvalues (arranged in descending order) and eigenvectors, respectively. Next, features having little information should be eliminated. Due to this, eigenvalues with $\frac{d_{(n,n)}}{d_{(1,1)}}$ lower than a threshold (assumed 10^{-13} here) and the associated eigenvectors should be eliminated. No eigenvalues and eigenvectors were eliminated here for the representative surface vectors. Finally, the transformation of the feature vectors will be performed using **Equation 13**.

$$Y = V^T X_{normalized} \quad (13)$$

Since the first component of the transformation keeps the most information, clustering will be performed using the first component of PCA.

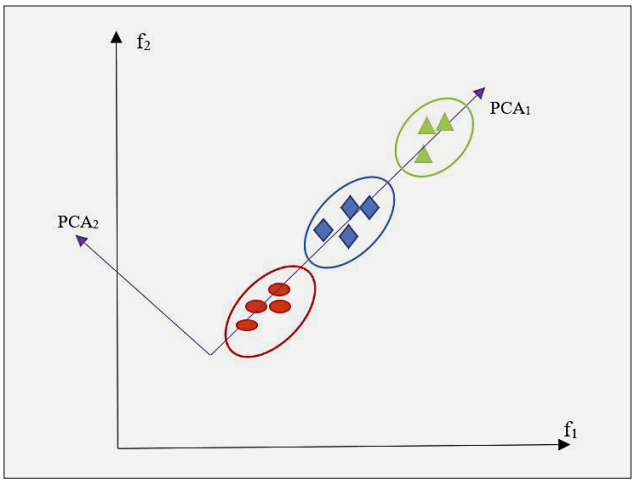

Figure 9: Schematic illustration of principal component analysis

6. Clustering

Different methods such as sequential, hierarchical, and optimization-based techniques have been developed for clustering a dataset (**Jain et al., 1999**). In this study, K-means, which is an optimization-based technique, will be used. Hence, a criterion function based on the squared error is applied which tends to work properly with compact and isolated clusters (**Equation 14**). Clustering is performed in four steps which are as follows (**Everitt et al., 2011**). First, cluster centers are selected. Then, each pattern is dedicated to the closest cluster center (the similarity measure for this purpose is Euclidean distance). Next, cluster centers will be updated. Finally, the process is repeated until the convergence criterion is fulfilled. Examples of the convergence criterion are the minimal reassignment of a pattern to a new cluster or increasing the criterion function. **Equation 14** presents the criterion function for pattern set ***Y*** and clustering ς:

$$e^2(Y, \varsigma) = \sum_{j=1}^{c_i} \sum_{i=1}^{n_j} \left\| y_i^j - C_j \right\|^2 \quad (14)$$

Where y_i^j is the i^{th} transformed representative feature vector belonging to the j^{th} cluster; C_i is the j^{th} cluster

center; c_t is the total number of clusters; n_i is the number of patterns in the j^{th} cluster. The method highly depends on the selection of the cluster centers and the number of clusters. Consequently, cluster centers were selected uniformly based on the dataset for reducing the former effect whereas the silhouette measure was used for decreasing the latter effect. Accordingly, clustering was performed for different cluster numbers (from 2 to 15 clusters). The clustering was repeated 200 times, and the best result (the minimum convergence function) is reported for each cluster number.

There are lots of measures by which the optimized number of clusters can be attained. To reach this goal, the silhouette measure was used in this study (**Rousseeuw, 1987**). This measure finds the optimal number of clusters according to the within cluster ($a_s(i)$) and between cluster distances ($b_s(i)$) (as illustrated in **Figure 10**) defined in **Equations 15 & 16**, respectively. The number of clusters by which the maximum average silhouette value ($si(i)$) is obtained (**Equation 17**), is considered the optimal number of clusters.

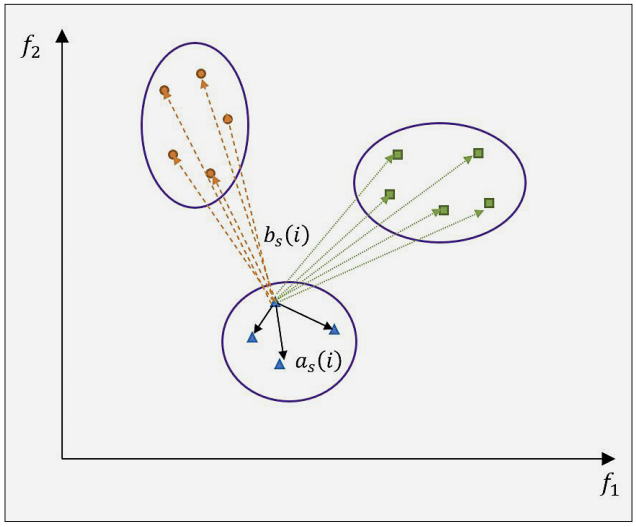

Figure 10: Schematic view of the parameters of the silhouette measure

$$a_s(i) = \frac{1}{|n_i|-1}\sum_{\substack{j\in I \\ i\neq j}} d_2(i,j) \tag{15}$$

$$b_s(i) = \min \frac{1}{|n_k|}\sum_{j\in K} d_2(i,j) \tag{16}$$

$$s(i) = \frac{b_s(i)-a_s(i)}{\max\{a_s(i), b_s(i)\}} \tag{17}$$

Where n_i is the number of patterns (transformed representative feature vectors) in the i^{th} cluster to which y_i belongs; n_k is the number of patterns in the k^{th} cluster to which y_i does not belong; $d_2(i,j)$ is the Euclidean distance between y_i and y_i patterns. **Table 1** shows average silhouette values ($s(i)$) for different cluster numbers. It demonstrates the fact that both methods of calculating surface representative vectors (mean and median), yield 13 optimized clusters. However, the representative median provides a little enhancement to the measure. Therefore, this technique was chosen for the comparison of the results with experiments, and a sample from each cluster is selected for conducting tests.

7. Experiments

Direct shear tests were performed on 13 selected samples for the calculation of the joint roughness coefficient (JRC). Hence, the upper part of the sample was encapsulated while the spilt spacer (clay) had fully covered the encapsulated lower part of the sample (**Muralha et al.,**

Table 1: The average silhouette value in each method of determining the surface representative vector

Number of clusters	Average silhouette value for clustering with representative mean vector	Average silhouette value for clustering with representative median vector
2	0.595	0.609
3	0.559	0.563
4	0.569	0.568
5	0.559	0.574
6	0.558	0.575
7	0.574	0.550
8	0.559	0.550
9	0.613	0.564
10	0.599	0.593
11	0.625	0.611
12	0.626	0.631
13	0.642	0.648
14	0.635	0.646
15	0.639	0.634

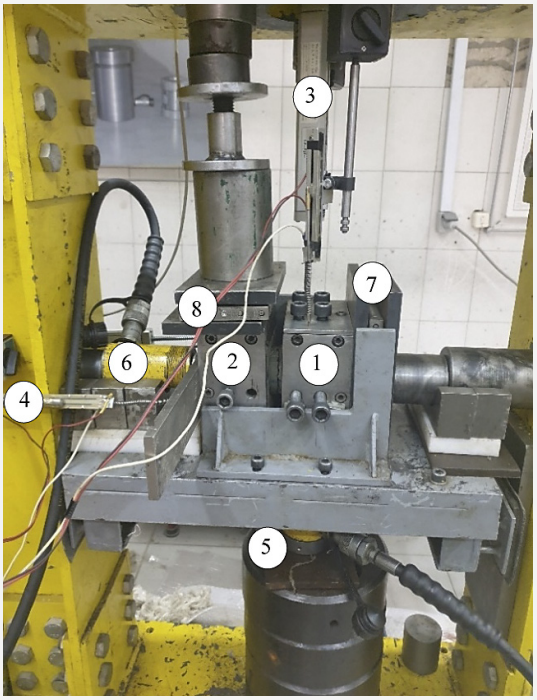

Number	Description
1	Movable box
2	Fixed box
3	Shear potentiometer
4	Normal potentiometer
5	Shear jack
6	Normal jack controlled by dead weight
7	Roller support for shear displacement
8	Roller support for normal displacement

Figure 11: Direct shear test setup for CNL condition

Table 2: The results of direct shear tests performed on selected samples

Cluster number	Number of samples in the cluster	$\sigma_n(Mpa)$	$\tau_p(Mpa)$	$JRC_{Back\ calculated}$
1	2	1.36	0.78	0.22
2	7	1.74	1.20	2.51
3	13	1.03	0.91	6.71
4	11	1.54	1.44	8.42
5	12	0.59	0.74	9.55
6	9	1.04	1.3	10.80
7	12	1.17	1.61	12.85
8	7	1.16	1.68	13.70
9	4	1.00	1.56	14.36
10	8	1.16	1.47	17.84
11	4	0.58	0.86	19.58
12	2	1.02	1.89	21.33
13	1	1.18	2.83	21.44

2014). Tests were performed in constant normal load (CNL) condition in which normal load was controlled by dead weight. The shear load was applied manually, and a long screw hydraulic pump was used to control the shearing rate. Shear and normal loads were recorded by pressure transducers (see **Figure 11**). Also, shear and normal displacements were recorded from the average of two potentiometers utilized in each direction. All the recorded data were gathered continuously by the data acquisition system.

The tests were conducted in a single step along the direction of the longer ellipse diameter (**Muralha et al., 2014**). The shear stress-shear displacement and normal displacement-shear displacement graphs were plotted for each sample (see **Figures 12 & 13**). The reduction of the surface contact during the test was also calculated and corrected according to (**Hencher and Richard, 1989**). JRC values are back-calculated using **Equation 18** (**Barton, and Choubey, 1977**).

$$\tau_p = \sigma_n . tan\left(\phi_r + JRC . log\left(\frac{JCS}{\sigma_n}\right)\right) \qquad (18)$$

Where τ_p is shear strength (*Mpa*); σ_n is normal stress (*Mpa*); JCS is the joint compressive strength (*Mpa*); ϕ_r is

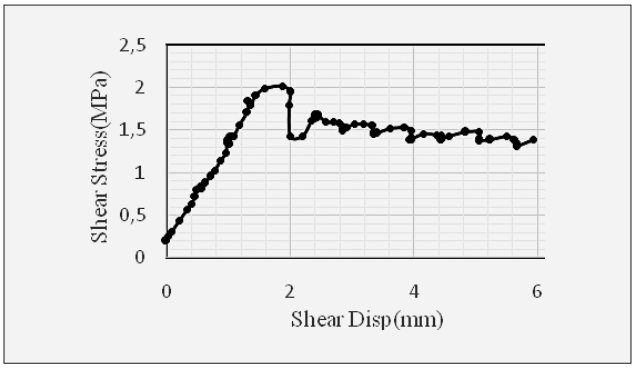

Figure 12: Shear stress-shear displacement graph recorded during the direct shear test

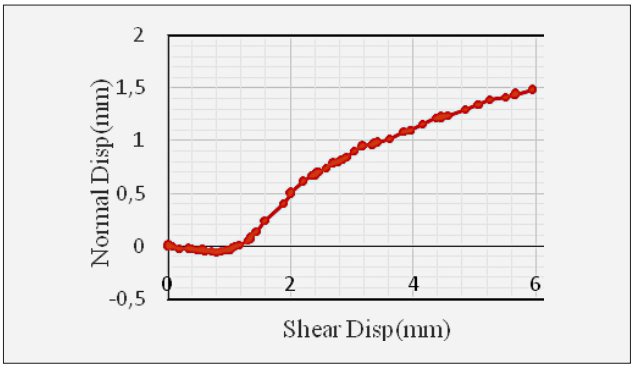

Figure 13: Normal displacement- shear displacement graph recorded during the direct shear test

Table 3 Representative feature vectors of the selected samples of clusters

Cluster Number	δ	λ	Z_2	$\frac{\theta^*_{max}}{1+C}$	$\frac{C_1}{a_1}$	$\left(\frac{\Delta L}{L_T}\right)_{FFT}$	*Pf*	PCA_1	$JRC_{Back\text{-}calculated}$
1	0.006	0.012	0.108	4.62	0.002	0.005	0.0016	-4.11	0.22
2	0.016	0.023	0.181	7.57	0.006	0.013	0.0051	-2.96	2.51
3	0.022	0.044	0.221	7.03	0.035	0.011	0.0148	-2.20	6.71
4	0.032	0.037	0.263	10.06	0.018	0.022	0.0213	-1.41	8.42
5	0.037	0.036	0.285	11.32	0.043	0.023	0.0213	-1.01	9.55
6	0.043	0.057	0.306	12.82	0.055	0.027	0.023	-0.20	10.8
7	0.054	0.071	0.344	14.18	0.060	0.027	0.037	0.67	12.85
8	0.052	0.076	0.334	14.97	0.088	0.028	0.038	0.93	13.70
9	0.065	0.075	0.384	15.49	0.113	0.034	0.0527	1.86	14.36
10	0.103	0.050	0.490	19.73	0.046	0.081	0.0376	3.42	17.84
11	0.098	0.093	0.492	19.31	0.165	0.040	0.0976	4.45	19.58
12	0.101	0.116	0.497	19.26	0.227	0.057	0.1187	5.89	21.33
13	0.143	0.145	0.626	27.17	0.349	0.043	0.1930	9.55	21.44

Table 4: Feature vectors of the profiles presented in **Figure 14**

Cluster Number	δ	λ	Z_2	$\frac{\theta^*_{max}}{1+C}$	$\frac{C_1}{a_1}$	$\left(\frac{\Delta L}{L_T}\right)_{FFT}$	*Pf*
1	0.006	0.012	0.108	4.83	0.0025	0.0049	0.0017
2	0.016	0.023	0.183	7.15	0.0081	0.0139	0.0055
3	0.018	0.043	0.200	6.79	0.0307	0.0136	0.0131
4	0.032	0.040	0.262	9.74	0.0185	0.0271	0.0159
5	0.034	0.035	0.281	11.14	0.0466	0.0230	0.0239
6	0.045	0.052	0.313	12.44	0.048	0.0275	0.0215
7	0.051	0.077	0.339	14.36	0.053	0.031	0.036
8	0.049	0.075	0.326	14.93	0.087	0.029	0.038
9	0.058	0.077	0.365	14.94	0.1218	0.0340	0.0514
10	0.102	0.047	0.487	19.73	0.0445	0.0809	0.0353
11	0.096	0.090	0.487	18.17	0.1741	0.0327	0.0944
12	0.098	0.108	0.469	19.49	0.2188	0.0572	0.1301
13	0.127	0.152	0.559	32.03	0.3267	0.0331	0.1688

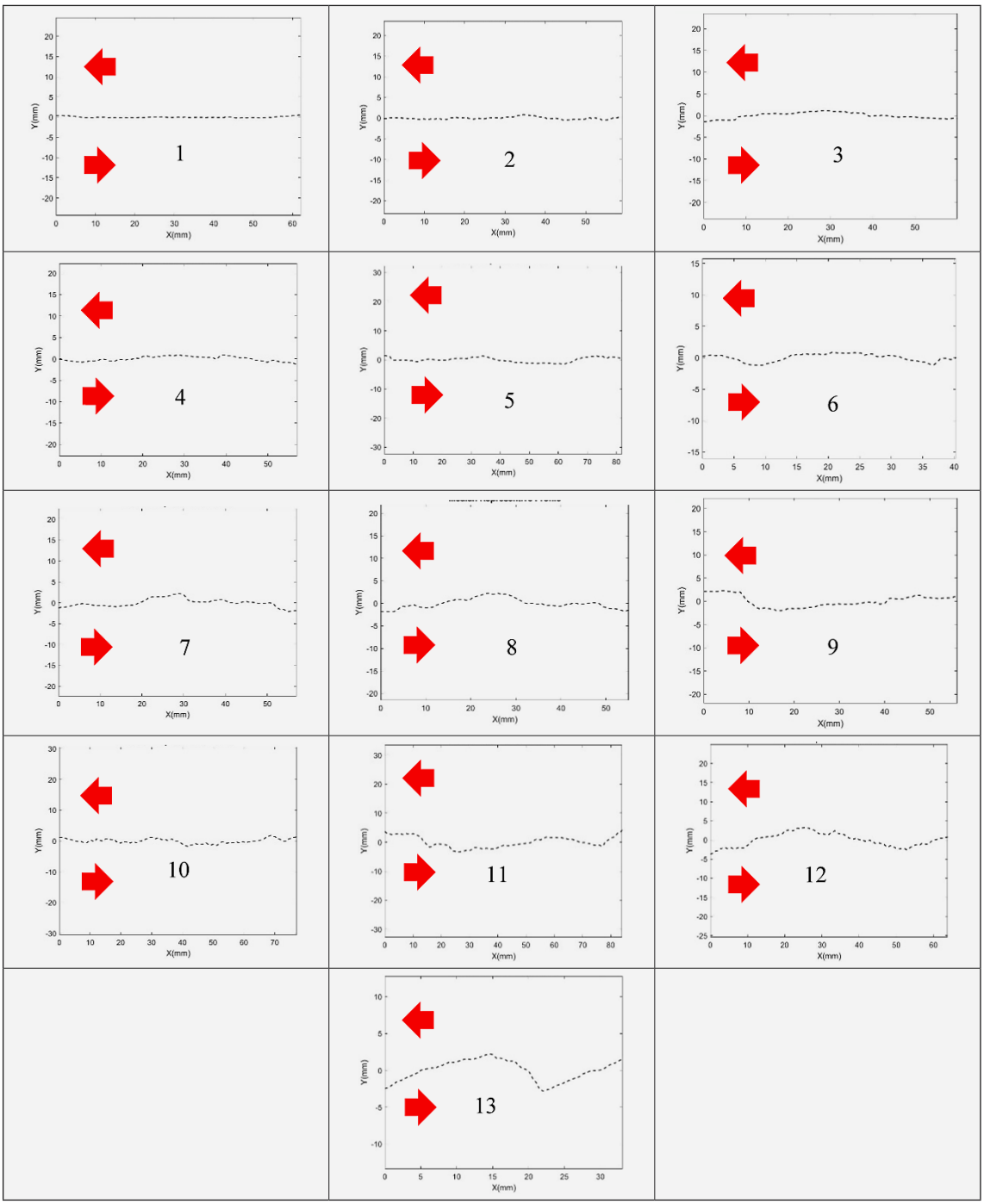

Figure 14: Profiles of the representative samples of clusters (arrows show the shear direction).

the residual friction angle (degrees) determined using **Equation 19** for weathered rock joints.

$$\phi_r = (\phi_b - 20) + 20\left(\frac{r}{R}\right) \quad (19)$$

Where ϕ_b is the basic friction angle (degrees); r is Schmidt rebound on a weathered joint surface (dimensionless); R is Schmidt rebound on an unweathered rock surface (dimensionless). The results of 13 direct shear tests performed on the selected samples were summarized in **Table 2** while it also shows the number of samples in each cluster. The normal stress in **Table 2** lies within the range 0.58-1.74 MPa which is a practical range for the stability analysis of rock slopes.

8. Comparison and Discussion

The representative feature vectors (derived from the median of the surface features) and the back-calculated JRCs for the selected samples of clusters were shown in **Table 3**. In addition, **Figure 14** illustrates the associated representative profiles, and **Table 4** demonstrates fea-

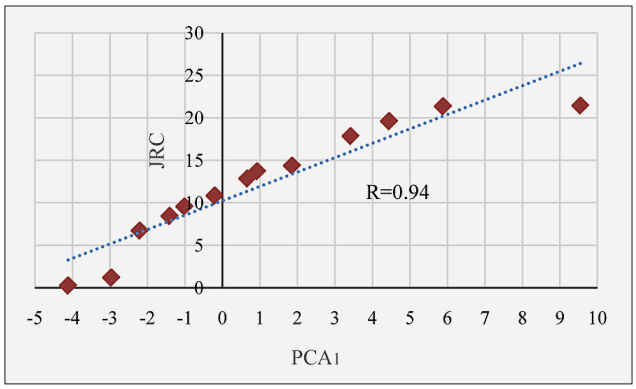

Figure 15: Relationship between the JRC and PCA_1 for the clusters presented in Table 3

tures of those profiles. The order of samples is based on the first component of *PCA* (which is called PCA_1), so the higher PCA_1, the rougher surface. The comparison of **Figure 14** and **Table 4** exhibits λ, $\frac{C_1}{a_1}$, Pf tend to show waviness while Z_2, $\frac{\theta^*_{max}}{1+C}$, $\left(\frac{\Delta L}{L_T}\right)_{FFT}$ lean toward unevenness, and is the combination of the both in a roughness profile.

Tables 3 & 4 reveal statistical, geostatistical, directional, and spectral features have an ascending trend although there are some exceptions. Consequently, using only a single parameter in order to describe surface roughness is not sufficient. In other words, more than one parameter should be selected such that the parameters properly indicate waviness and unevenness of a profile. This seems to be the most important reason for the disordering of the parameters that has been reported for Barton standard profiles (**Gao et al., 2015; Jang et al., 2014; Tatone and Grasselli, 2013; Lianheng et al., 2018; Pickerin and Aydin, 2015; Asadi et al., 2010**). Nevertheless, PCA_1 in which the waviness and unevenness of a profile are combined using the features, varies uniformly. **Figure 15** depicts the relationship between the JRC and PCA_1 for the clusters presented in **Table 3** demonstrating a strong correlation (R=0.94). Thus, PCA_1 reflects the roughness level of the surfaces.

Comparing the JRC values back-calculated from test results with the order presented in **Tables 3 & 4** shows that even though the general trend of the JRC values adapts to those obtained from pattern recognition analysis, the results might be affected by two important sources that are the rebound value of the Schmidt hammer on rough surfaces and the experimental basis of the Barton model. The effect of weathering is incorporated into the model through residual friction angle and joint compressive strength, both of which are calculated based on Schmidt rebound values. However, the rebound values of the Schmidt hammer highly depend on morphology of the sample. Indeed, surface irregularities might cause an unexpected reduction of the values (**Aydin, 2008**). Another source affecting the back-calculated JRCs is the experimental basis of the Barton model providing an approximation of surface roughness. Therefore, the arguments imply that the back-calculated JRCs might not be accurate enough for the exact determination of surface roughness.

9. Conclusion

In this study, clustering of the joint surfaces was performed based on a pattern recognition procedure using statistical, geostatistical, directional, and spectral features. The proposed approach groups samples with almost similar JRC values using a systematic recognition of rock surfaces that relies on profile features describing the waviness and unevenness of the surface. Hence, 92 natural joint surfaces producing more than 10,000 profiles were scanned, and δ, λ, Z_2, $\frac{C_1}{a_1}$, $\frac{\theta^*_{max}}{1+C}$, $(\Delta L)_{FFT}$, Pf parameters were calculated for all the surface profiles. While λ, $\frac{C_1}{a}$, Pf manifest waviness, Z_2, $\frac{\theta^*_{max}}{1+C}$, $\left(\frac{\Delta L}{L_T}\right)_{FFT}$ reveal unevenness of the profiles, and δ is the combination of them both.

The representative vector of a surface was calculated using the weighted mean and median of the profile features. Similarly, the representative profile of a surface was selected as the one closest to the representative vector. Thus, the representative surface vector and profile were introduced based on a quantitative procedure.

Principal component analysis (PCA) was implemented for the combination of the different features so that the directions with high-level information were assigned. In addition, the K-means was used for the clustering of the natural joint surfaces using the first component of the *PCA* analysis. Furthermore, the silhouette measure was applied in order to find the optimal number of clusters. The measure shows compared to the weighted mean, clustering of the surface roughness using the weighted median provides better cluster separation, and 13 clusters were assigned as the optimal number of clusters.

Assessing the representative features of the selected samples demonstrates although statistical, geostatistical, directional, and spectral features might seldom change in a non-uniform manner, PCA_1 varies uniformly. Therefore, this parameter was chosen as a reference in order to evaluate the surface roughness of samples.

Comparing the back-calculated JRCs of the selected samples with the results of clustering (PCA_1 of the clusters) shows the two have a good agreement (correlation coefficient = 0.94) though the results might be affected by the rebound values of the Schmidt hammer on rough surfaces and the experimental basis of the Barton criterion.

The approach can be applied for surface roughness quantification provided that all the samples are scanned with the same sampling interval (attention should be

paid to too large or too small sampling intervals resulting in neglecting or exaggerating irregularities of the surface, respectively). Furthermore, since the features are influenced by the scale effect, the proposed clustering method can be used on the condition that the samples have almost the same size.

The results revealed using only a single parameter for the recognition of a rough surface is not sufficient. Consequently, a number of features showing the waviness and unevenness of a surface should be selected. This procedure was followed in this study and it resulted in a quantitative recognition of surface roughness.

Acknowledgement

The authors wish to acknowledge Mr. Kazemi and Farsijani, from the Regional Water Company of Tehran, and Mr. Besharatniya, Aldavaher and Vahedi from Mahabghodss Company for their assistance to supply the samples for this study.

References

Ankah, M.L.Y., Sunkpal, D.T., Zhao, X. and Kulatilake, P.H.S.W. (2022): Role of heterogeneity on joint size effect, and influence of anisotropy and sampling interval on rock joint roughness quantification. Geomechanics and Geophysics for Geo-Energy and Geo-Resources 8, 101. https://doi.org/10.1007/s40948-022-00413-2

Asadi, M. S., Rasouli, V. and Tokhmechi, B. (2010): Wavelet analysis of JRC exemplar profiles. Rock Engineering in Difficult Ground Conditions – Soft Rocks and Karst, 215-220, London, United Kingdom.

Askari, M. and Ahmadi, M. (2007): Failure process after peak strength of artificial joints by fractal dimension, Geotechnical and Geological Engineering, 25, 631–637. http:// doi.org/10.1007/s10706-007-9135-6

Aydin, A. (2008): ISRM suggested method for determination of the Schmidt hammer rebound hardness: revised version. In: Ulusay R. (eds) The ISRM Suggested Methods for Rock Characterization, Testing and Monitoring, 2007-2014. Springer, Cham. http:// doi.org/10.1016/j.ijrmms.2008.01.020

Bae, D., Kim, K., Koh, Y. and Kim, J. (2011): Characterization of joint roughness in granite by applying the scan circle technique to images from a borehole televiewer. Rock Mechanics and Rock Engineering, 44, 497–504. http:// doi.org/10.1007/s00603-011-0134-9

Barton N. and Choubey, V., (1977): The shear strength of rock joints in theory and practice. Rock Mechanics, 10, 1–54. http://doi.org/10.1007/BF01261801

Barton, N., Wang, C. and Yong, R. (2023): Advances in joint roughness coefficient (JRC) and its engineering applications. Journal of Rock Mechanics and Geotechnical Engineering, Article in Press.

Chen, S.J., Zhu, W.C., Yu, Q.L. and Liu, X.G. (2016): Characterization of anisotropy of joint surface roughness and aperture by variogram approach based on digital image processing technique, Rock Mechanics and Rock Engineering, 26, 855–876. http:// doi.org/10.1007/s00603-015-0795-x

Cormen, Th.H., Leiserson, Ch.E., Rivest, R.L. and Stein, C. (2001): Introduction to Algorithms, The MIT Press, Massachusetts, 499 p.

Duda, R., Hart, P. E. and Stork, D. (2001): Pattern Classification, Wiley (2nd edition), New York, 688 p.

Everitt, B.S., Landau, S., Leese, M. and Stahl, D. (2011): Cluster Analysis, Wiley Series in Probability and Statistic, United Kingdom, 352 p.

Fathipour-Azar, H. (2021): Data-driven estimation of joint roughness coefficient. Journal of Rock Mechanics and Geotechnical Engineering, 13, 1428-1437. https://doi.org/10.1016/j.jrmge.2021.09.003

Feder, J. (1988): Fractals, Plenum Press, New York.

Gao, Y., Ngai, L., Wong, Y. (2015): A modified correlation between roughness parameter Z_2 and the JRC. Rock Mechanics and Rock Engineering, 48, 387-396. http:// doi.org/10.1007/s00603-013-0505-5

Grasselli, G. and Egger, P. (2003): Constitutive law for the shear strength of rock joints based on three-dimensional surface parameters. International Journal of Rock Mechanics and Mining Sciences, 40, 25–40. http://doi.org/10.1016/S1365-1609(02)00101-6

Grasselli, G., Wirth, J. and Egger, P. (2002): Quantitative three-dimensional description of a rough surface and parameter evolution with shearing. International Journal of Rock Mechanics and Mining Sciences, 39, 789–800. https://doi.org/10.1016/S1365-1609(02)00070-9

Hencher, S.R., and Richard, L.R. (1989): Laboratory direct shear testing of rock discontinuities. Ground Engineering, 22, 24-31.

ISRM Suggested methods for the quantitative description of discontinuities in rock masses. International Journal of Rock Mechanics and Mining Sciences, 1978, 15, 319–68. https://doi.org/10.1016/0148-9062(78)91472-9

Jain, A.K., Murty, M.N. and Flynn, P.J. (1999): Data clustering: a review, ACM Computing Surveys, 31(3), 264-323. http:// doi.org/10.1145/331499.331504

Jang, H., Kang, S., Jang, B. (2014): Determination of joint roughness coefficients using roughness parameters, Rock Mechanics and Rock Engineering, 47, 2061-2073. http:// doi.org/10.1007/s00603-013-0535-z

Jansson, S., (2006): Evaluation of Methods for Estimating Fractal Properties of Intensity Images, Master of Science Thesis, Ume°a University, Sweden.

Kulatilake, P.H.S.W. and Ankah, M.L.Y. (2023): Rock joint roughness measurement and quantification – A review of the current status. Geotechnics, 3(2), 116-141. https://doi.org/10.3390/geotechnics3020008

Kulatilake, P.H.S.W. and Um, J. (1998): Requirements for accurate quantification of self-affine roughness using the variogram method. International Journal of Solids and Structures, 35, 4167-4189. http:// doi.org/10.1016/S0020-7683(97)00308-9.

Kulatilake, P.H.S.W. and Um, J. (1999). Requirement for accurate quantification of self-affine roughness using the roughness–length method. International Journal of Rock

Mechanics and Mining Sciences, 36, 5–18. http:// doi.org/10.1016/S0148-9062(98)00170-3.

Kulatilake, P.H.S.W., Shou, G., Huang, T. H. and Morgan, R.M. (1995): New peak shear strength criteria for anisotropic rock joints. International Journal of Rock Mechanics and Mining Sciences and Geomechanics Abstracts, 32, 673-697.

Kulatilake, P.H.S.W., Um, J. and Pan, G. (1997): Requirements for accurate quantification of self-affine roughness using the line scaling method. Rock Mechanics and Rock Engineering, 30, 171-206. http:// doi.org/10.1007/BF010 45716

Ladanyi, B. and Archambault, G. (1970): Simulation of the shear behavior of a jointed rock mass. Proceedings of the 11th U.S. Symposium on Rock Mechanics, 7,105-125.

Lee, Y. H., Carr, J.R., Barr, D.J. and Haas, C.J. (1990): The fractal dimension as a measure of the roughness of rock discontinuity profilesInternational Journal of Rock Mechanics and Mining Sciences and Geomechanics Abstracts, 27(6), 453-464. http:// doi.org/10.1016/0148-9062(90)90998-H

Li, Y. and Zhang, Y. (2015): Quantitative estimation of joint roughness coefficient using statistical parameters. International Journal of Rock Mechanics and Mining Sciences, 77, 27–35. http://doi.org/10.1016/j.ijrmms.2015.03.016

Lianheng Zh., Shuaihao, Zh., Dongliang, H., Shi, Z. and Dejian, L. (2018): Quantitative characterization of joint roughness based on semivariogram parameters, International Journal of Rock Mechanics and Mining Sciences, 109,1-8. http:// doi.org/10.1016/j.ijrmms.2018.06.008

Liu, Q., Tian, Y., Ji, P. and Ma, H. (2018): Experimental investigation of the peak shear strength criterion based on three-dimensional surface description. Rock Mechanics and Rock Engineering, 51:1001-1025. http:// doi.org/10.1007/s00603-017-1390-0

Magsipoc, E., Zhao, Q. and Grasselli, G. (2020): 2D and 3D roughness characterization. Rock Mech Rock Eng, 53, 1495-1519. http:// doi.org/10.1007/s00603-019-01977-4

Mandelbrot, B.B. (1983): The fractal geometry of nature, Freeman, San Francisco, 460 p.

Muralha, J., Grasselli, G., Tatone, B., Blumel, M, Chryssanthakis, P. and Yujing, J. (2014), ISRM suggested method for laboratory Determination of the shear strength of rock joints: revised version. Rock Mechanics and Rock Engineering, 47, 291–302. http:// doi.org/10.1007/s00603-013-0519-z

Patton, F.D.)1966(: Multiple modes of shear failure in rock. 1st Congress of International Society of Rock Mechanics, 1: 509-513.

Pickerin, C. and Aydin, A. (2016): Modeling roughness of rock discontinuity surfaces: a signal analysis approach. Rock Mechanics and Rock Engineering, 49, 2959-2965. http:// doi.org/10.1007/s00603-015-0870-3

Pierra, J., Parisi Baradad, V., Garsia Ladona, E., Lombarte, A., Recasense, L. and Cabestany, J. (2005): Otolith shape feature extraction oriented to automatic classification with open distributed data, Marine and Fresh Water Research, 56,805-814.

Poon, C.Y., Sayles, R.S. and Jones, T.A. (1992): Surface measurement and fractal characterization of naturally fractured rocks. Journal of Physics D: Applied Physics, 25,1269-1275. http:// doi.org/10.1088/0022-3727/25/8/019

Roko, R.O., Daemenj, J.J.K. and Myers, D.E. (1997): Variogram characterization of joint surface morphology and asperity deformation during shearing. International Journal of Rock Mechanics and Mining Sciences, 34(1), 71–84. http:// doi.org/10.1016/S1365-1609(97)80034-2

Rousseeuw, P.J. (1987): Silhouettes: a Graphical Aid to the Interpretation and Validation of Cluster Analysis. Computational and applied Mathematics, 20, 53–65. https://doi.org/10.1016/0377-0427(87)90125-7

Shirono, T. and Kulatilake, P.H.S.W. (1997): Accuracy of the spectral method in estimating fractal/spectral parameters for self-affine roughness profiles. International Journal of Rock Mechanics and Mining Sciences and Geomechanics Abstracts, 34, 789-804. http:// doi.org/10.1016/S1365-1609(96)00068-X

Sun, G.Z., (1988): Structural Mechanics of Rock Mass. (Chinese). Beijing, China: Scientific Press. https://doi.org/10.1007/978-94-011-6501-3_3

Tang, Z.C. and Wong, L.N.Y. (2015): New criterion for evaluating the peak shear strength of rock joints under different contact states. Rock Mechanics and Rock Engineering, 49, 1191–1199. http:// doi.org/10.1007/s00603-015-0811-1

Tatone, B.S.A. and Grasselli, G. (2010): A new 2D discontinuity roughness parameter and its correlation with JRC. International Journal of Rock Mechanics and Mining Sciences, 47(8), 1391–1400. http:// doi.org/10.1016/j.ijrmms.2010.06.006

Tatone, B.S.A. and Grasselli, G. (2013): An investigation of discontinuity roughness scale dependency using high-resolution surface measurements. Rock Mechanics and Rock Engineering, 46, 657-681. https://doi.org/10.1007/s00603-012-0294-2

Tse, R. and Cruden, D.M. (1979): Estimating joint roughness coefficients. International Journal of Rock Mechanics and Mining Sciences and Geomechanics Abstracts, 16, 303–7. http:// doi.org/10.1016/0148-9062(79)90241-9.

Ueng, T.S. and Chang, W.C. (1990): Shear strength of joint surface profiles. Symposium on Rock Mechanics (USRMS). American Rock Mechanics Association. http:// doi.org/10.1201/9781003078944-38

Wang, C., Wang, L. and Karakus, M. (2019): A new spectral analysis method for determining the joint roughness coefficient of rock joints. International Journal of Rock Mechanics and Mining Sciences, 113, 72–82. http://doi.org/10.1016/j.ijrmms.2018.11.009

Wang, L., Wang, C., Khoshnevisan, S., Ge, Y. and Sun, Z. (2017): Determination of two-dimensional joint roughness coefficient using support vector regression and factor analysis. Engineering Geology, 231, 238-251. https://doi.org/10.1016/j.enggeo.2017.09.010

Xia, C.C., Tang, Z.C., Xiao, W.M. and Song, Y.L. (2014): New peak shear strength criterion of rock joints based on quantified surface description. Rock Mechanics and Rock Engineering, 47(2), 387–400. http:// doi.org/10.1007/s00603-013-0395-6.

Xie, H.P. and Pariseau, W.G., (1994): Fractal estimation of rock joint roughness coefficient. Science China, 24(5), 524–530.

Yang, J., Rong, G., Hou, D., Peng, J. and Zhou, C. (2016): Experimental study on peak shear strength criterion for rock joints. Rock Mechanics and Rock Engineering, 49, 821-835. http:// doi.org/10.1007/s00603-015-0791-1

Yang, Z.Y., Lo, S.C. and Di, C.C. (2001): Reassessing the joint roughness coefficient (JRC) estimation using Z_2. Rock Mechanics and Rock Engineering, 34, 243–51. http:// doi.org/10.1007/s006030170012

Yong, R., Ye, J., Li, B. and Du, S.G. (2018): Determining the maximum sampling interval in rock joint roughness measurements using Fourier series. International Journal of Rock Mechanics and Mining Sciences, 101,78-88. http:// doi.org/10.1016/J.IJRMMS.2017.11.008

Yu, X.B. and Vayssade, B. (1991): Joint profiles and their roughness parameters. International Journal of Rock Mechanics and Mining Sciences and Geomechanics Abstracts, 28, 333–336. http:// doi.org/10.1016/0148-9062 (91)90598-G

Zhang, G.C., Karakus, M., Tang, H.M., Ge, Y.F. and Zhang. L. (2014): A new method estimating the 2D joint roughness coefficient for discontinueity surfaces in rock masses. International Journal of Rock Mechanics and Mining Sciences, 72,191–198. http:// doi.org/10.1016/j.ijrmms.2014.09.009

Zhang, X., Jiang, Q., Chen, N., Wei, W. and Feng, X. (2016): Laboratory investigation on shear behavior of rock joints and a new peak shear strength criterion. Rock Mechanics and Rock Engineering, 49, 3495–3512. http:// doi.org/10.1007/s00603-016-1012-2

Zhao, J. (1997b): Joint surface matching and shear strength. Part B: JRC-JMC shear strength criterion. International Journal of Rock Mechanics and Mining Sciences and Geomechanics Abstracts, 34, 179-185. http://doi.org/10.1016/S0148-9062(96)00063-0

SAŽETAK

Procjena hrapavosti površine prirodnih stijenskih pukotina temeljena na tehnici nenadziranog prepoznavanja uzoraka pomoću 2D profila

Stabilnost raspucane stijenske mase općenito se kontrolira posmičnom čvrstoćom koja značajno ovisi o hrapavosti površine. Do sada su prikazane različite metode za određivanje hrapavosti površine pomoću 2D profila. U ovom radu predlaže se nova metoda koja se temelji na tehnici nenadziranog prepoznavanja uzoraka kombinacijom statističkih, geostatističkih, usmjerenih i spektralnih metoda za kvantifikaciju hrapavosti površine. Kako bi se postigao taj cilj, skenirano je više od 10.000 profila prikupljenih s 92 površine prirodnih stijenskih pukotina. Uzorci su prikupljeni iz vapnenačkih jezgri brane Lar koja se nalazi u pokrajini Mazandaran u Iranu. Nakon uvođenja novog spektralnog indeksa, određenog Fourierovom transformacijom za mjerenje neravnina hrapavih profila, izvučene su statističke, geostatističke, usmjerene i spektralne značajke koje opisuju valovitost i neravnine 2D profila, a reprezentativni vektor i profil za svaku površinu uvedeni su kroz ponderiranu aritmetičku sredinu i medijan značajki profila. Analiza glavnih komponenti (PCA) korištena je za pronalaženje smjera najvećeg odstupanja informacija. Zatim je grupiranje 92 uzorka provedeno putem metode K-sredina, a mjera siluete korištena je kako bi se pronašao optimalan broj grupa, a to je rezultiralo stvaranjem 13 grupa. Za provjeru postupka odabran je uzorak u svakoj grupi, a na tim uzorcima provedena su ispitivanja izravnog smicanja. Usporedba rezultata ispitivanja i grupiranja pokazala je dobro slaganje, stoga je ova metoda učinkovit alat za kvantitativno utvrđivanje hrapavosti s obzirom na valovitost i neravnine površine.

Ključne riječi:
koeficijent hrapavosti pukotina; posmična čvrstoća pukotina; prepoznavanje uzoraka; grupiranje; analiza glavnih komponenti.

Author Contributions

Ali Mohamad Pakdaman (Ph.D. Candidate of Mining Engineering) carried out the pattern recognition analyses, performed the laboratory tests, prepared the results, and wrote the manuscript under the guidance and supervision of **Mahdi Moosavi** (Professor of Mining Engineering) who provided the interpretations and presentation of the results. Both the authors read and approved the final manuscript.